



22/02/2022

Design of *In Situ* Cathodic Charging of TMCP Steel under Flexural Loading

Sarah Hiew¹, Bostjan Bezensek², Steve Paterson², Willem Maarten van Haaften³,
Thibaut Dessolier¹, Stella Pedrazzini¹ & Ben Britton¹

¹ Department of Materials, Imperial College, Exhibition Rd, London, SW7 2AZ, UK

² Shell Global Solutions UK, 1 Altens Farm Road, Aberdeen, AB12 3YF, UK

³ Shell Global Solutions International BV, Grasweg 31, 1031HW Amsterdam, The Netherlands



- Ben Wood, Ruth Birch, Aigerim Omirkhan and Abigail Ackerman from Department of Materials, Imperial College London
- P S Marsden (Precision Engineers) Ltd
- David Miller and Harry Barnett from Advance Hackspace, Imperial College London
- Matt Moderate the Health and Safety Technical Officer of Imperial College London

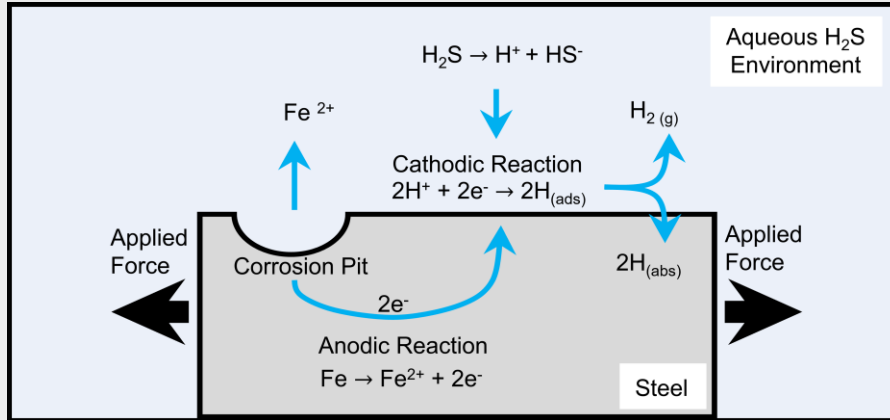


Figure 1. Schematic shows hydrogen absorption process in steel within aqueous H₂S environment. [adapted from T.S.Chong et al., *Engineering Fracture Mechanics*, (2014)]

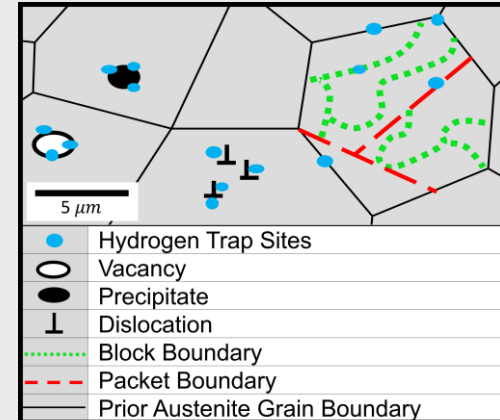


Figure 2. Schematic shows hydrogen traps within microstructure of TMCP steel. [adapted from F. Vucko et al., *Eurocorr*, (2013)]

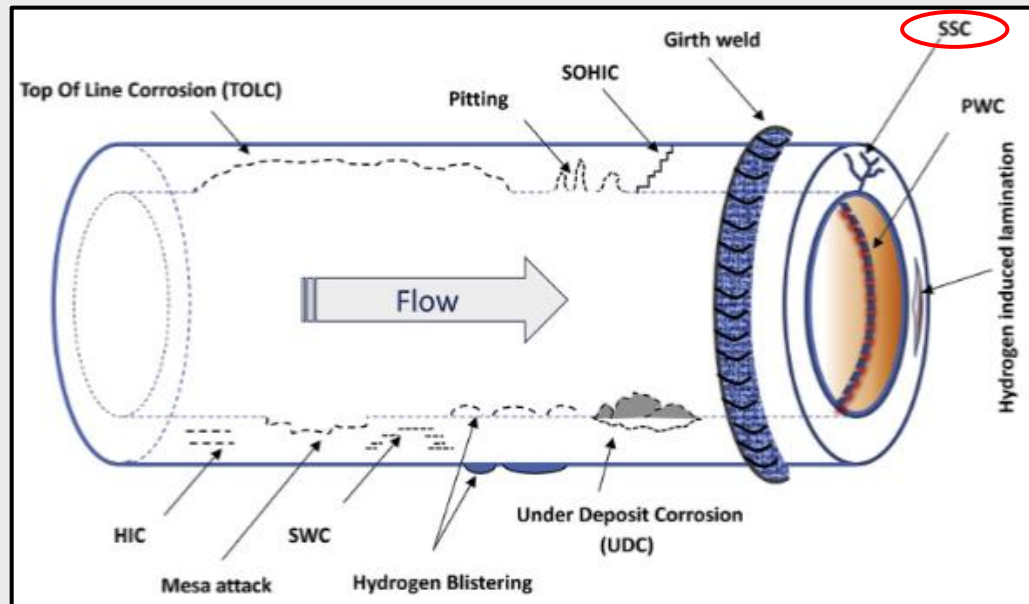


Figure 3. Schematic of different forms of defects in hydrocarbon pipelines. [M. Askari. et al., *J. Nat. Gas. Sci. Eng.*, (2019)]



- Minimum yield strength of 65 ksi (i.e. approximately 449 MPa)
- Tensile strength of 531 MPa
- Thermo-mechanical control process (TMCP) = Thermomechanical Rolling + Accelerated Cooling
- Cooled via mild accelerated cooling (MAC) [1]

Table 1. Composition of As Given X-65 TMCP Material.

	Fe	C	Si	Mn	P	S	Cu	Ni	Cr	Nb	Ti	Al	Ca
At (%)	94.535	0.230	0.471	1.386	0.016	0.001	0.182	0.150	0.244	0.011	0.013	0.008	2.753

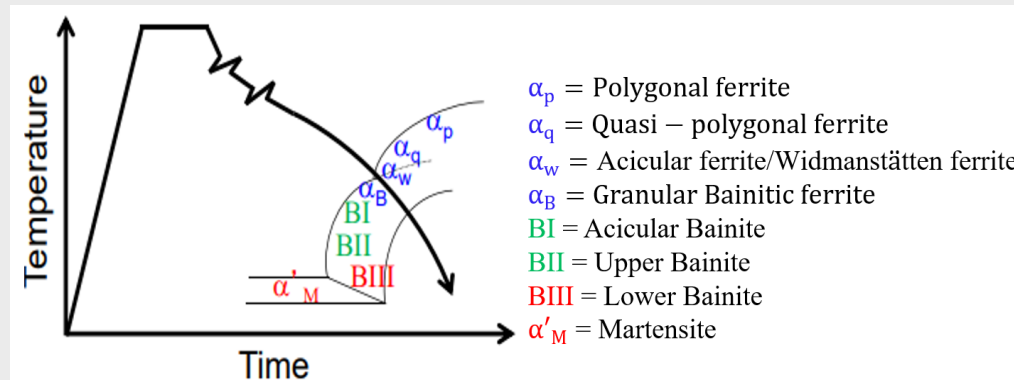


Figure 4. Schematic drawing of processing route of as received TMCP material on a TTT diagram. [Nippon Steel Corporation, (2020)]

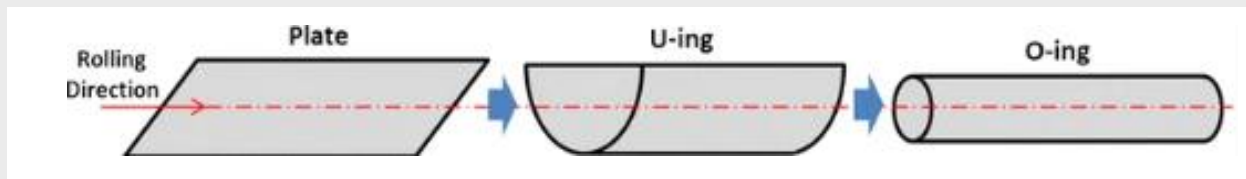


Figure 5. Schematic diagram showing the UOE process in fabricating TMCP steel pipes where the rolling direction of TMCP plate parallel to longitudinal direction of pipe section. [S. Y. Shin., Metall. Mater. Trans. A Phys., (2013)]

[1] Y. Shinohara et al., "Development of a high strength steel line pipe for strain-based design applications," in *The Seventeenth International Offshore and Polar Engineering Conference*, Jul. 2007, pp. 2949–2954.



- What microstructural features would effect SSC propagation?

Prior Austenite Grain Boundaries

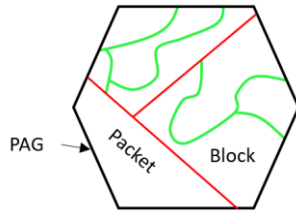


Figure 6. Schematic diagram shows the different coloured grain boundaries for the different hierarchy of features within a prior austenite grain.

- SSC tends to propagate along PAG boundaries [1]
- PAG boundaries are mostly HAGBs [1]
- HAGB has a higher hydrogen binding energy [2]
- PAG reconstruction GUI [3]

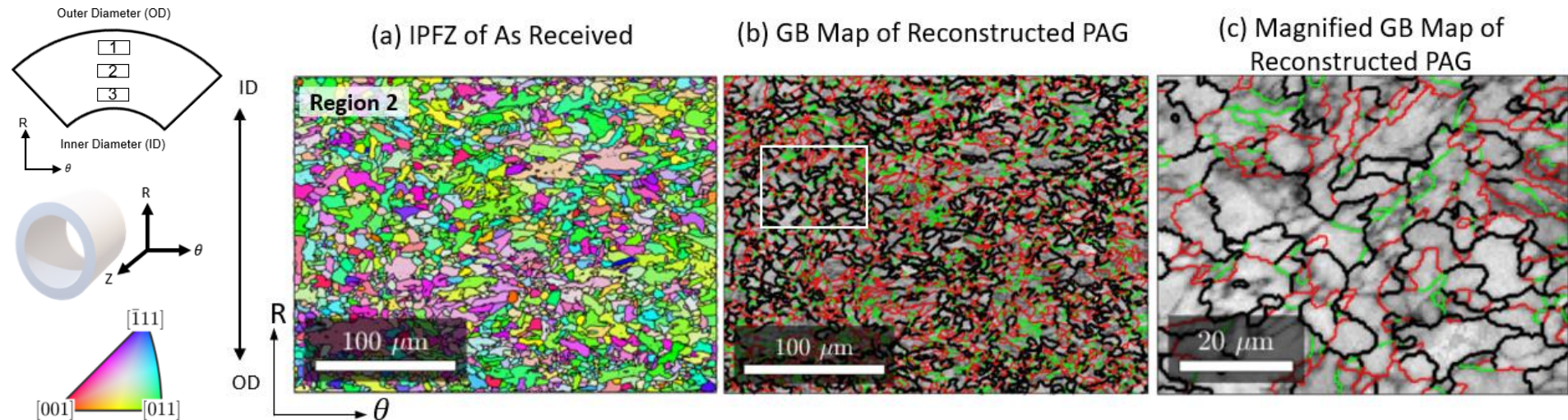


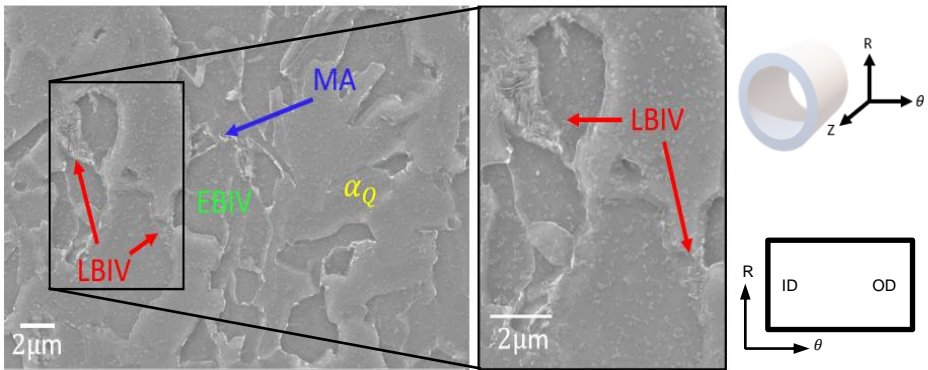
Figure 7. (a) Inverse Pole Figure (IPF) of mean orientation map for grains taken along Z direction of pipe from region 2 shown in schematic on the left, (b) grain boundary map of reconstructed PAG and (c) the respective magnified images taken from regions highlighted by white shown from left to right .

[1] A. Nagao, C. D. Smith, M. Dadfarnia, P. Sofronis, and I. M. Robertson, "Interpretation of hydrogen-induced fracture surface morphologies for lath martensitic steel," *Procedia Mater. Sci.*, vol. 3, pp. 1700–1705, Jan. 2014, doi: 10.1016/j.mspro.2014.06.274.
 [2] W. T. Read and W. Shockley, "Dislocation models of crystal grain boundaries," *Phys. Rev.*, vol. 78, no. 3, p. 289, May 1950, doi: 10.1103/PhysRev.78.275.
 [3] T. Nyyssönen, M. Isakov, P. Peura, and V.-T. Kuokkala, "Iterative Determination of the Orientation Relationship Between Austenite and Martensite from a Large Amount of Grain Pair Misorientations" *Metall. Mater. Trans. A*, vol. 47 (6), pp. 2587–2590, 2016.



- What microstructural features would effect SSC propagation?

Phases Observed



MA= Martensite-Austenite Constituents

α_Q = Quasi-polygonal ferrite
EBIV= Equiaxed granular bainite
LBIV= Lath-like granular bainite



Figure 8. Nitral etched sample taken from near outer diameter of the pipe section and a magnified region outlined by a black rectangle. Image taken using backscattered electron mode using an electron beam of 20kV.

1) Proportion of MA

- Harder martensite than surrounding phases.
- Induced transformation of retained austenite into martensite.

2) Morphology of MA

- Blocky MA have less chance of delaying propagation of SSC.
- Thin film perpendicular to crack direction reduce propagation but promote interfacial debonding.

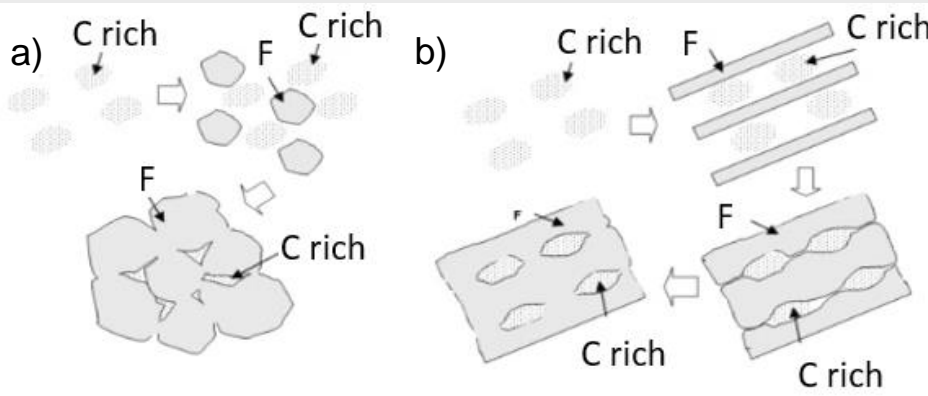


Figure 9. Schematic diagram shows transformation process of two different granular bainite morphology: a) equiaxed granular bainite and b) lath-like granular bainite. [Z. X. Qiao et al., J. Alloys Compd., (2009)]

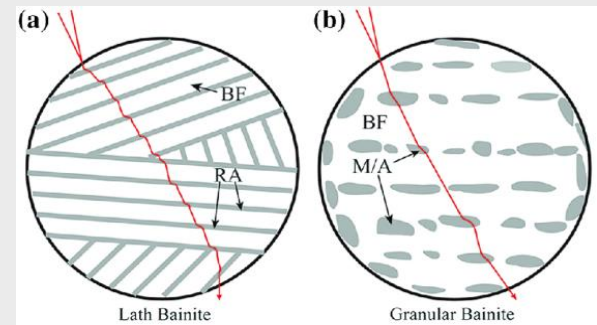


Figure 10. Schematic diagram comparing crack propagation indicated by red line through a) lath-like bainite consisting bainitic ferrite (BF) and retained austenite (RA) films and b) granular bainite containing BF and martensite-retained austenite (MA) islands. [X. Chen. et al., Min. Met. Mat. Series., (2019)]



High Pressure H₂S Autoclave System

e.g. NACE standard industrial test TM0177 and TM0316

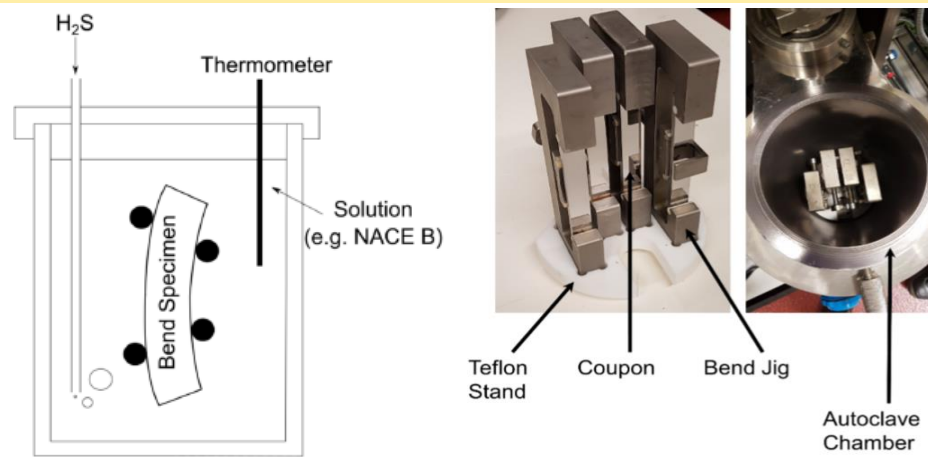


Figure 11. Photo and schematic diagram of the four-point bend jigs placed in the autoclave chamber [Jim Hickey, PhD Thesis, (2019)]

New *in situ* cathodic charging

- Advantages:
 - ✓ Less hazardous to operator
 - ✓ Shorter test duration and reduced set-up cost
 - ✓ Versatile for *in situ* non-destructive measurements
- Limitations:
 - ✗ Restricted to ambient temperature and pressure.
 - ✗ Restricted to flexural loading (i.e. three-point bend under fixed strain rate in this case).

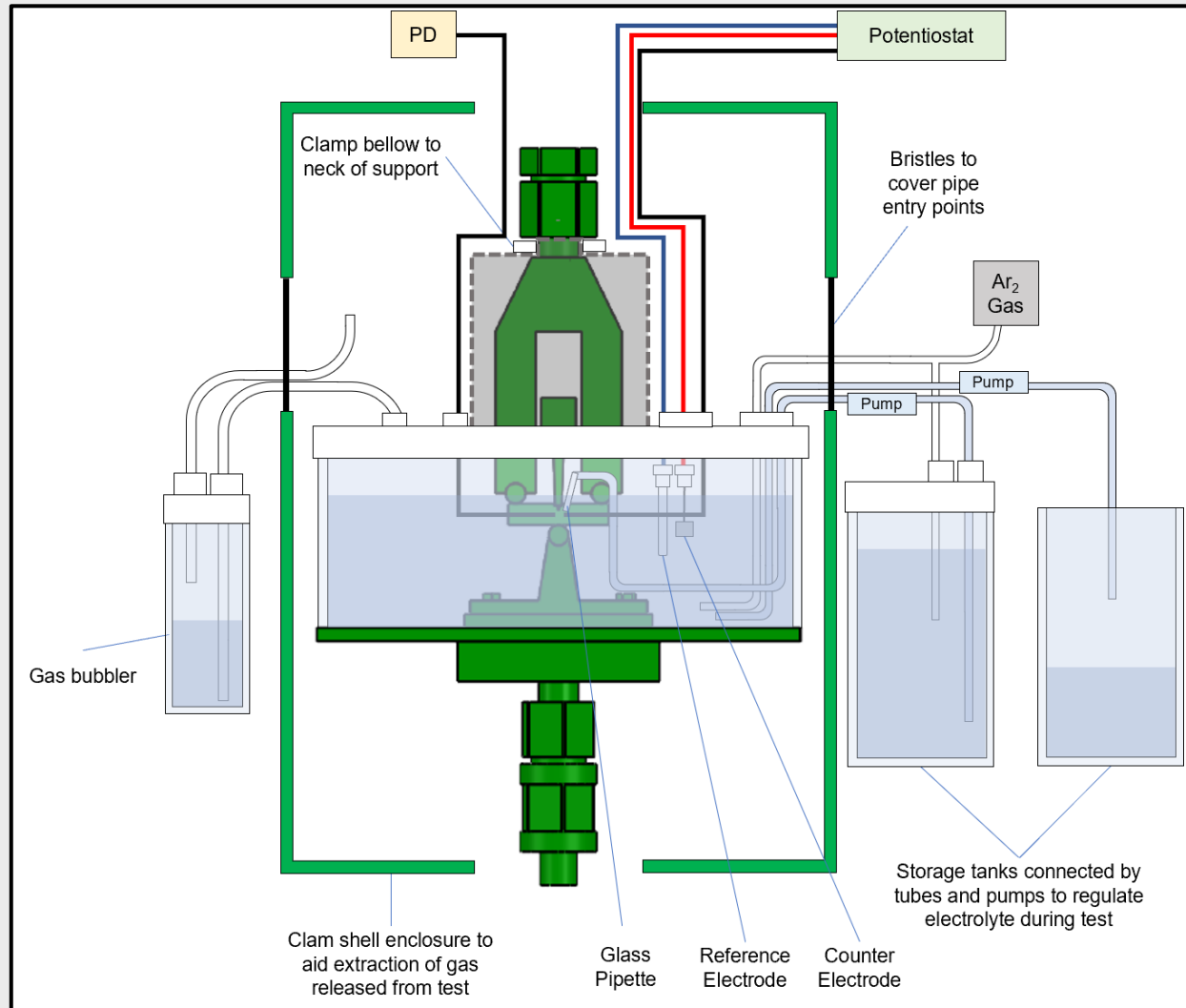


Figure 12. Schematic diagram of *in situ* cathodic charging rig design which sits on 100kN Mayes servo-hydraulic machine. Components currently available indicated in green.

Features of *in situ* cathodic charging rig set-up:

- 1) Three-point bending rig**
 - Allow ease of containment of electrolyte.
 - Ensure pure flexural bending mode.
- 2) Circulation of electrolyte**
 - Regulate the concentration of electrolyte.
- 3) Enclosure**
 - Aid extraction of gas released.
- 4) Three different crack monitoring techniques:**
 - These three techniques shall complement each other.
 - a) Clip Gauge
 - b) Direct Current Potential Drop (DCPD)
 - c) 2D-Optical Digital Imaging Correlation (DIC)



Three Point Bend Rig Assembly

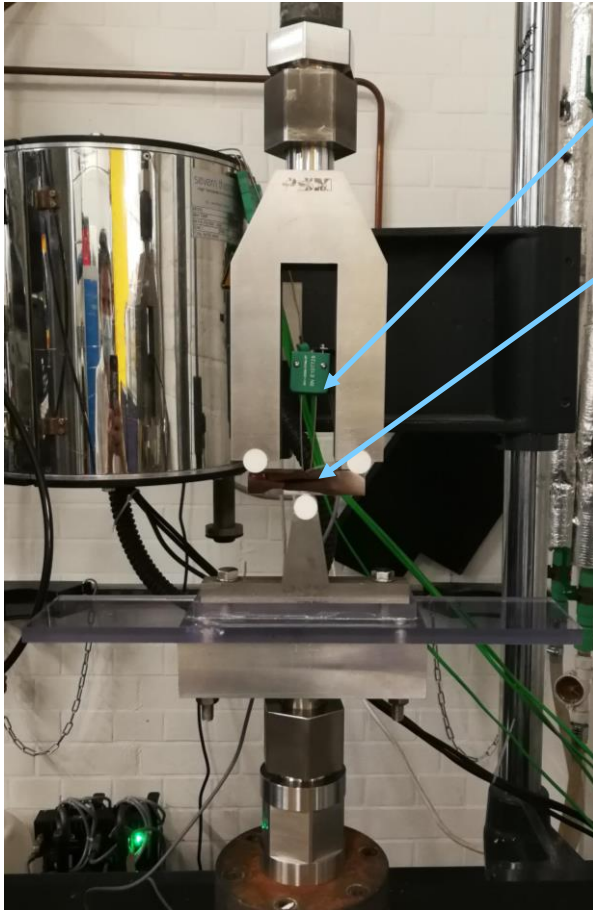


Figure 13. Photo showing 3 point bend rig setup on servo-hydraulic test machine with clip gauge in place for pre-cracking of notched CTOD sample .

Clip gauge

Pre-crack Notched Three Point Bend Sample



Figure 14. Photo shows notched sample deformed during pre-cracking test.

Optical Set up for Digital Image Correlation



Figure 15. Photo shows CCD camera and inspection tube arrangement.



Figure 16. Video showing filtered images of crack in sample captured by optical camera over the duration of pre-crack.

Table 2. Comparison Crack Measurement Techniques for In Situ Mechanical Testing & Cathodic Charging

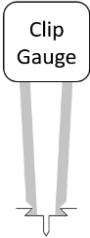
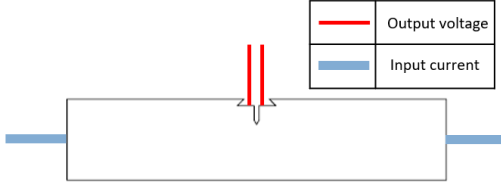
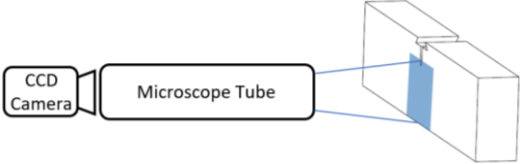
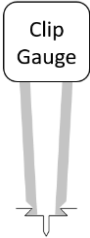
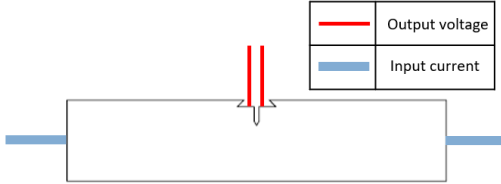
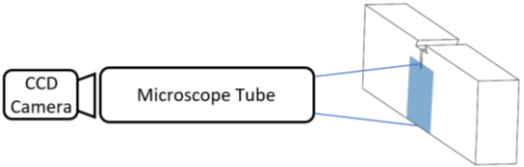
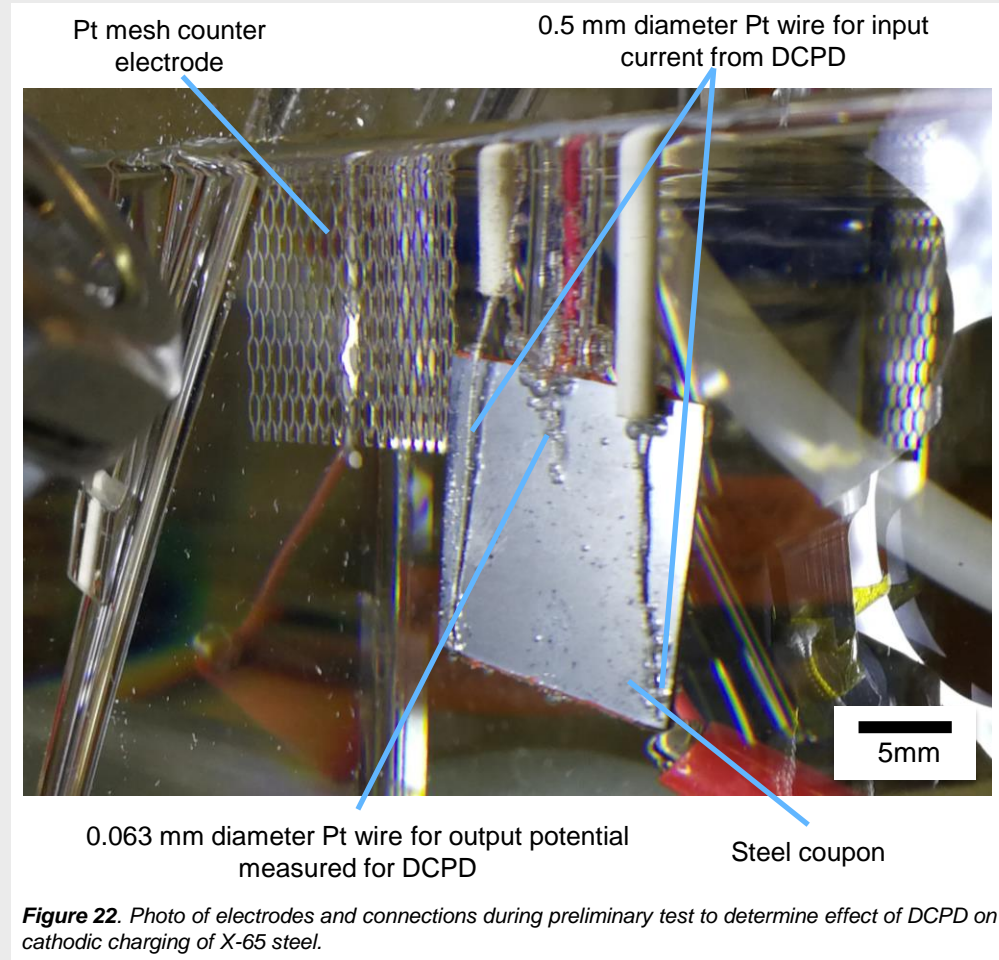
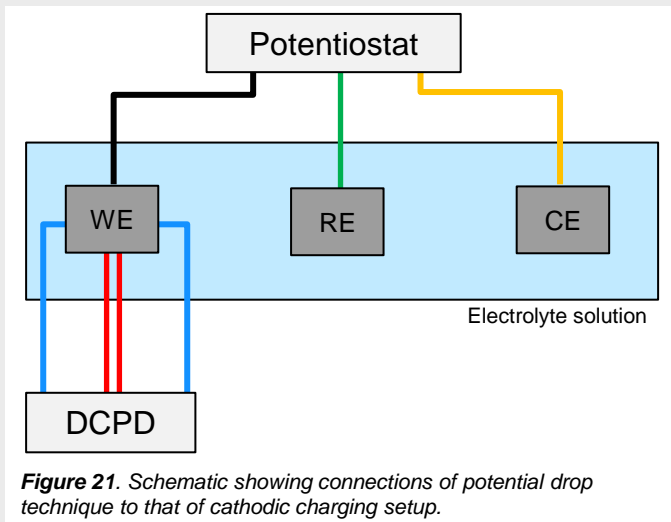
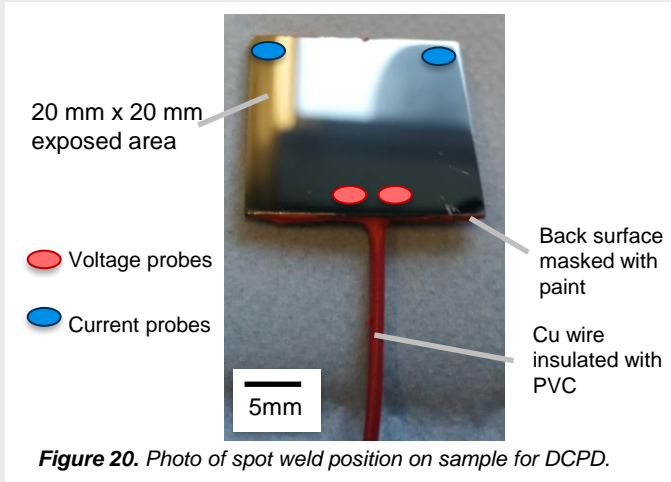
Non-Destructive Crack Measurement Techniques	Crack Tip Opening Displacement (CTOD)	Direct Current Potential Drop (DCPD)	Digital Image Correlation (DIC)
<p>Brief Description</p>	<p>Notch mouth opening measured via clip gauge.</p>  <p><i>Figure 17. Schematic showing clip gauge and knife edges attached on single edge notched bend sample.</i></p>	<p>Changes in resistance measured and correlated with crack extension. (via potential drop measurements)</p>  <p><i>Figure 18. Schematic showing probe locations on sample for DCPD measurements.</i></p>	<p>2D full field strain measurement. Track surface displacements using time-series of optical micrographs and surface patterning</p>  <p><i>Figure 19. Schematic showing optical DIC setup.</i></p>
<p>Advantage</p>	<ul style="list-style-type: none"> • Mechanically simple to use, and commonly employed. • Does not interfere with cathodic charging system. 	<ul style="list-style-type: none"> • Provides crack extension information rather than notch opening displacement. 	<ul style="list-style-type: none"> • Non-contact and does not interfere with cathodic charging. • Observe full field strains, displacements and crack opening.
<p>Disadvantage</p>	<ul style="list-style-type: none"> • Does not provides spatial resolution of crack propagation. • Indirect relationship of CTOD and crack extension. 	<ul style="list-style-type: none"> • Simple model used for correlation of length and voltage drop. • No spatial resolution. • Requires electrical contacts on the sample, leading to localised corrosion. • Current applied to conductive sample may interfere with the charging condition. 	<ul style="list-style-type: none"> • Hydrogen bubbles occlude regions. • Care with patterning method and local surface microstructure & electrochemistry.

Table 2. Comparison Crack Measurement Techniques for In Situ Mechanical Testing & Cathodic Charging

Non-Destructive Crack Measurement Techniques	Crack Tip Opening Displacement (CTOD)	Direct Current Potential Drop (DCPD)	Digital Image Correlation (DIC)
<p>Brief Description</p>	<p>Notch mouth opening measured via clip gauge.</p>  <p><i>Figure 17. Schematic showing clip gauge and knife edges attached on single edge notched bend sample.</i></p>	<p>Changes in resistance measured and correlated with crack extension. (via potential drop measurements)</p>  <p><i>Figure 18. Schematic showing probe locations on sample for DCPD measurements.</i></p>	<p>2D full field strain measurement. Track surface displacements using time-series of optical micrographs and surface patterning</p>  <p><i>Figure 19. Schematic showing optical DIC setup.</i></p>
<p>Advantage</p>	<ul style="list-style-type: none"> • Mechanically simple to use, and commonly employed. • Does not interfere with cathodic charging system. 	<ul style="list-style-type: none"> • Provides crack extension information rather than notch opening displacement. 	<ul style="list-style-type: none"> • Non-contact and does not interfere with cathodic charging. • Observe full field strains, displacements and crack opening.
<p>Disadvantage</p>	<ul style="list-style-type: none"> • Does not provides spatial resolution of crack propagation. • Indirect relationship of CTOD and crack extension. <p>(1)</p>	<ul style="list-style-type: none"> • Simple model used for correlation of length voltage drop. • No spatial resolution. • Requires electrical contacts on the sample, leading to localised corrosion. • Current applied to conductive sample may interfere with the charging condition. <p>(2)</p>	<ul style="list-style-type: none"> • Hydrogen bubbles occlude regions. • Care with patterning method and local surface microstructure & electrochemistry.

(1) Direct Current Potential Drop (DCPD)

- Investigate the effect of applied current from DCPD on cathodic charging of sample.



(1) Direct Current Potential Drop (DCPD)

- Investigate the effect of applied current from DCPD on cathodic charging of sample.

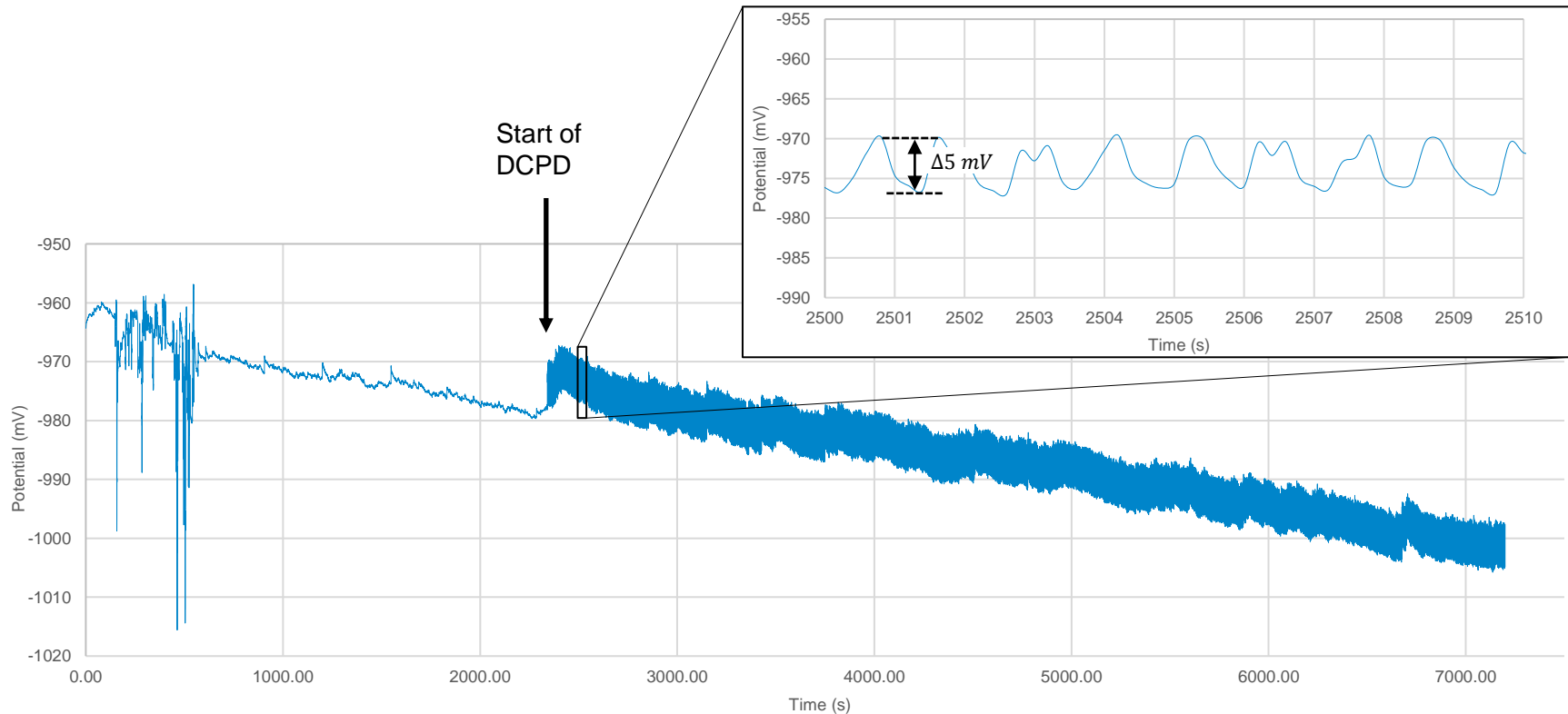


Figure 23. Potential measured from potentiostat over 2hrs of cathodic charging of 2cm^2 X-65 exposed area using $0.2\text{M H}_2\text{SO}_4 + 3\text{g/L NH}_4\text{SCN}$ electrolyte where -5mA was applied.

- 5mA applied from potentiostat.
- 5A current was pulsed approximately every 1 second to reduce thermal junction effect and reduce localised corrosion effect at welded contact points [1].

(2) 2D-Optical Digital Imaging Correlation (DIC)

- Overcome bubbles formed in field of view cathodic charging process.

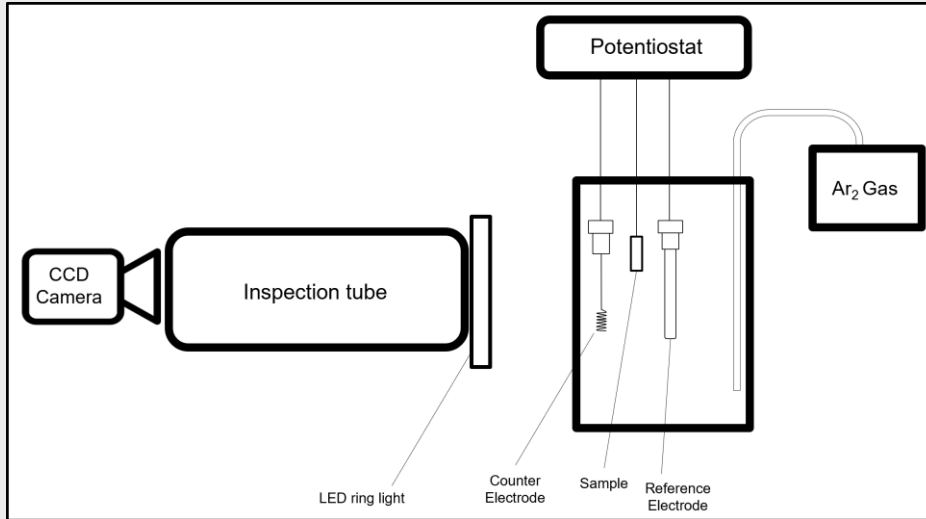


Figure 24. Schematic diagram showing inspection tube with CCD camera set-up for in situ observation of sample surface under cathodic charging.

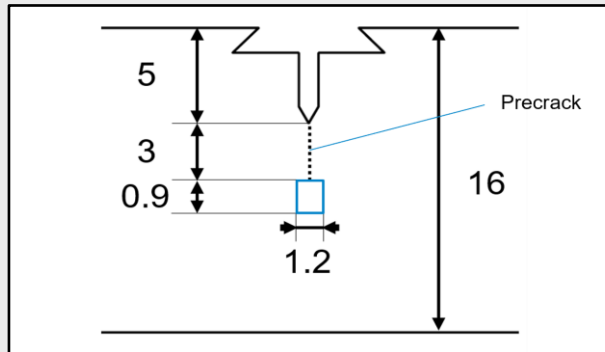


Figure 25. Schematic diagram comparing the field of view from video shown in Figure 26 on a 3pt bend notched sample where dimensions annotated are in mm.

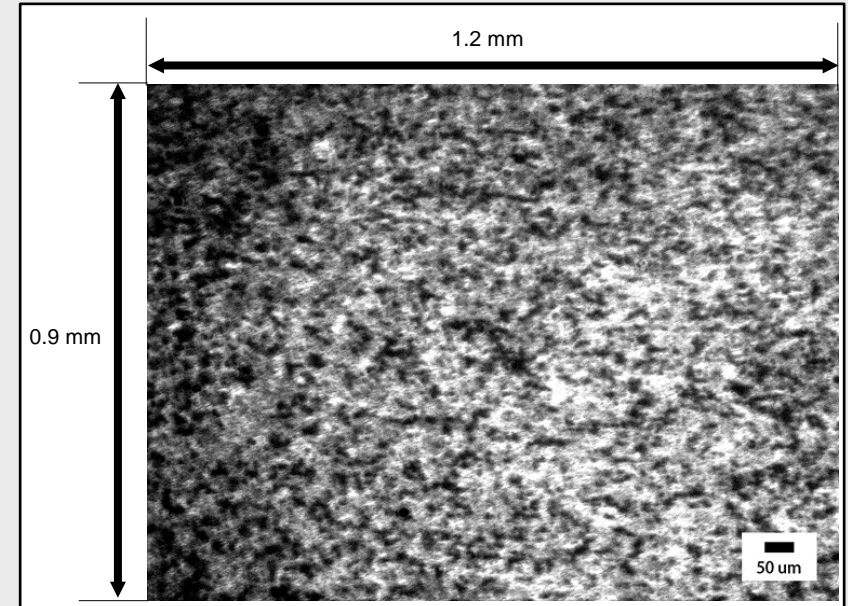


Figure 26. Video showing optical images of sample surface charged with -5 mA/cm^2 current density, using $0.2 \text{ M H}_2\text{SO}_4 + 3\text{g/L NH}_4\text{SCN}$ for the first 16 mins.

(2) 2D-Optical Digital Imaging Correlation (DIC)

- Overcome bubbles formed in field of view cathodic charging process.

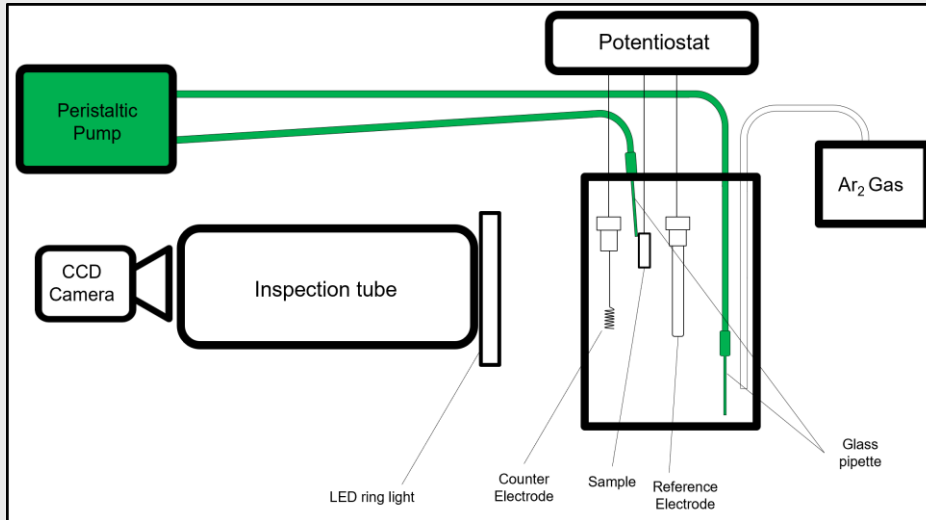


Figure 27. Components highlighted in green were added to recirculate solution, and implement the stream on sample surface in attempt to remove bubbles formed.

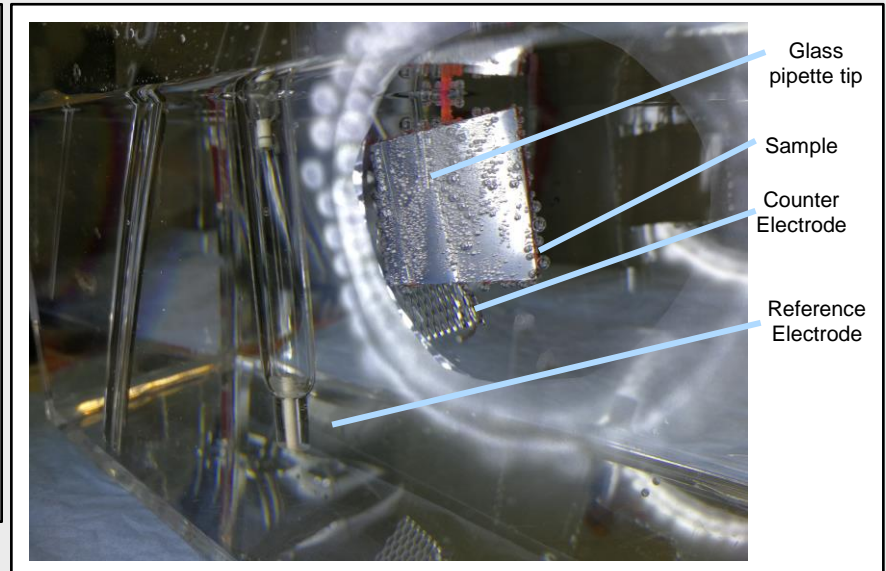


Figure 28. Zoomed in photo showing recirculation of cathodic charging solution set up to form a path of bubble - free region on sample surface.

- Does increased movement of solution across surface effect hydrogen adsorption?

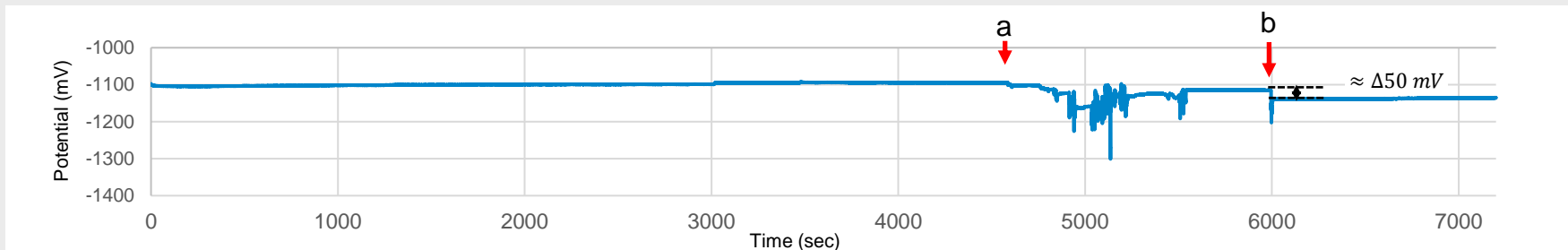


Figure 29. Potential recorded over 2hrs of cathodic charging with -5mA/cm^2 current density using $0.2\text{ M H}_2\text{SO}_4 + 3\text{g/L NH}_4\text{SCN}$.

- Speed of pump = 50 rpm
 - Flow rate = 42ml/min (this was the max)
- Glass pipette tip

1.4mm \varnothing

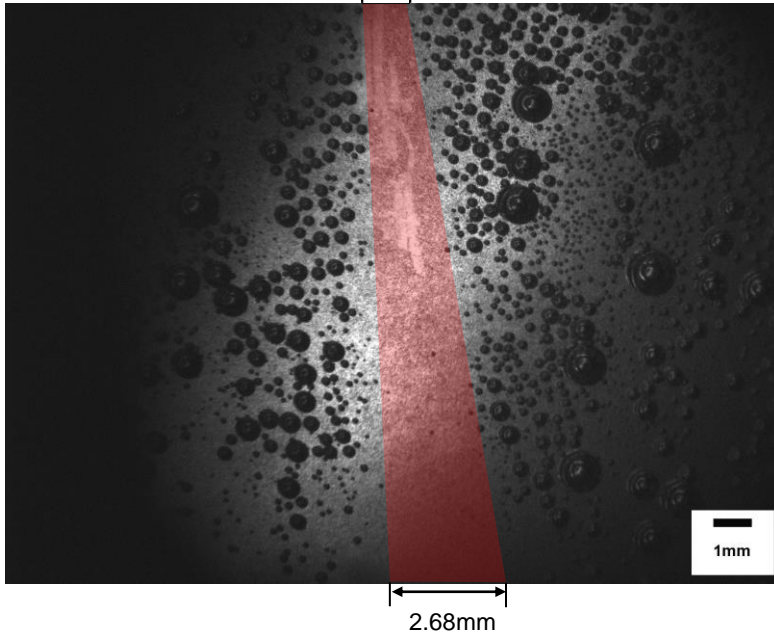


Figure 30. Red shading highlights bubble-free region on speckled preliminary coupons.

- If using the same flow settings on single edged notched bend sample...

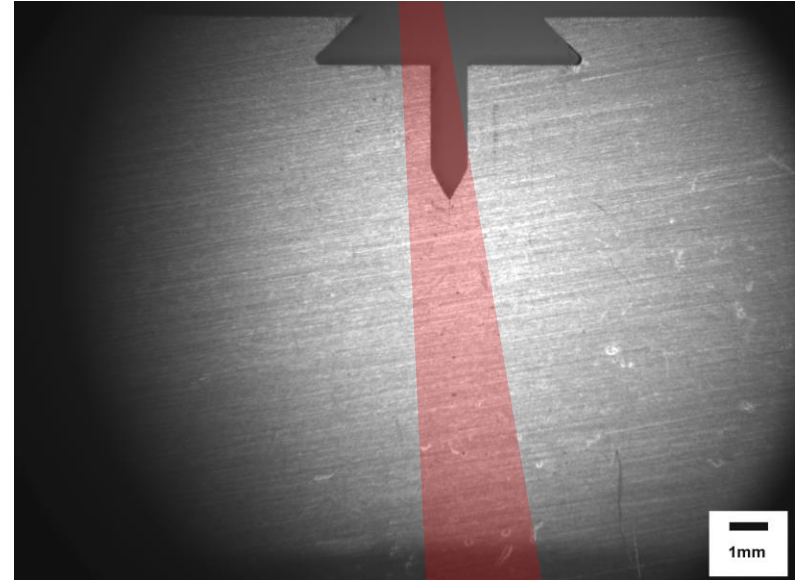


Figure 31. Red shading highlights area of bubble-free region expected on single edged notched bend sample.



Summary

- New *in situ* cathodic charging set-up has been designed to understand the microstructure mechanisms of HE in TMCP steels.
- Three complementary crack opening measurement methods developed to enable correlation of hydrogen transport and crack propagation.

Next Steps

- Relate lab-based electrochemical testing to in-service like conditions
 - (a) Correlate [H] and time constants, via permeability testing.
 - (b) Compare electrochemical tests with autoclave tests.
- Use high resolution characterisation methods to explore mechanisms of crack propagation during hydrogen charging, e.g. varying strain rate/peak load for pre-crack.



22/02/2022

Thank you

Sarah Hiew¹, Bostjan Bezensek², Steve Paterson², Willem Maarten van Haften³,
Thibaut Dessolier¹, Stella Pedrazzini¹ & Ben Britton¹

¹ Department of Materials, Imperial College, Exhibition Rd, London, SW7 2AZ, UK

² Shell Global Solutions UK, 1 Altens Farm Road, Aberdeen, AB12 3YF, UK

³ Shell Global Solutions International BV, Grasweg 31, 1031HW Amsterdam, The Netherlands